Magnetic resonance in the chiral helimagnet $CrNb_3S_6$

Daichi Yoshizawa[1,2], Jun-ichiro Kishine[2,3], Yusuke Kousaka[2,4],
Yoshihiko Togawa[2,5], Masaki Mito[2,6], Jun Akimitsu[2,4,7], Katsuya Inoue[2,4]
and Masayuki Hagiwara[1,2]

[1]*Center for Advanced High Magnetic Field of Science, Graduate School of Science,
Osaka University, Toyonaka, Osaka 560-0043, Japan*
[2]*Center for Chiral Science, Hiroshima University, Higashihirosima, Hiroshima 739-8526, Japan*
[3]*Division of Natural and Environmental Science, The Open University of Japan, Mihama,
Chiba 261-8586, Japan*
[4]*Graduate School of Science, Hiroshima University, Higashihiroshima,
Hiroshima 739-8526, Japan*
[5]*Department of Physics and Electronics, Osaka Prefecture University, Sakai,
Osaka 599-8531, Japan*
[6]*Faculty of Engineering, Kyusyu Institute of Technology, Kitakyushu, Fukuoka, Japan*
[7]*Department of Physics and Mathematics, Aoyama-Gakuin University, Sagamihara,
Kanagawa 252-5258, Japan*

yoshizawa@mag.ahmf.sci.osaka-u.ac.jp, kishine@ouj.ac.jp, koyu@hiroshima-u.ac.jp, y-
togawa@pe.osakafu-u.ac.jp, mitoh.masaki540@mail.kyutech.jp, jun@phys.aoyama.ac.jp,
kxi@hiroshima-u.ac.jp, hagiwara@ahmf.sci.osaka-u.ac.jp

Abstract

Recently, magnetic substances with chirality, namely the handedness of the magnetic structure, have attracted considerable attention because of the anomalous phenomena which appear in magnetic fields. $CrNb_3S_6$ is one of the chiral magnets formed by exchange and Dzyaloshinsky-Moriya (DM) interactions. Electron spin resonance (ESR) measurements of $CrNb_3S_6$ in magnetic fields parallel to the c-axis (helical axis) have been performed to evaluate the exchange and the DM constants that determine the helical structure. Fitting the ESR data to a calculated mode based on a spin wave theory yields values for the ferromagnetic inter-plane exchange constant $J/k_B = 16.2$ K, the DM constant $D/k_B = 1.29$ K, and the single-ion anisotropy constant $K_\perp/k_B = 1.02$ K. From the Curie-Weiss temperature $\theta_{CW} \sim 145$ K, large intra-plane ferromagnetic exchange interactions are suggested.

Keywords: Chiral magnet, Electron spin resonance, Dzyaloshinsky-Moriya interaction, exchange interaction

1 Introduction

Helical magnetic structure sometimes causes intriguing magnetic and electronic properties. A cycloidal spin structure is a kind of helical spin texture, and the helical plane lies parallel to the modulation vector of the spin helical structure. TbMnO$_3$ [1, 2] and CuO$_2$ ribbon chain systems [3, 4] with this magnetic structure, in which the antiferromagnetic and ferroelectric transitions occur simultaneously, have indicated multiferroic behavior, and the relation $\boldsymbol{P} \propto \boldsymbol{Q} \times \boldsymbol{e}_3$ holds in these materials, where $\boldsymbol{P}$, $\boldsymbol{Q}$, and $\boldsymbol{e}_3$ are the ferroelectric polarization, the helical axis, and the modulation vector of the spin helical structure, respectively [5]. Because of the cross-correlation relation between magnetism and electricity, compounds with a helical magnetic structure have attracted much attention.

The origins of such helical magnetic structures are categorized into two types. One of them is the competition between the nearest-neighbor (NN) and the next-nearest-neighbor (NNN) exchange interactions ("symmetric" helimagnets). Most helical magnetic states which appeared in TbMnO$_3$ [2], the CuO$_2$ ribbon chain system [6, 7], and the rare-earth materials [8] are explained by this origin. The other origin is the Dzyaloshinsky-Moriya (DM) interaction ("chiral" helimagnets). An asymmetric crystal structure, in which no inversion symmetry exists between neighboring magnetic ions, gives rise to the DM interaction through the relativistic spin-orbit coupling, and a chiral helimagnetic structure appears when the DM vector is uniform in the system.

The chiral helimagnets show some intriguing features in magnetic fields. One example of such a chiral helimagnet is CsCuCl$_3$, which belongs to the $P6_122$ or $P6_522$ space group [9]. The neutron diffraction measurements revealed that the magnetic structure of CsCuCl$_3$ below T_N=10.5 K is helical and is caused by the ferromagnetic intra-chain interaction and the DM interaction, where the DM vector is parallel to the c-axis (the helical axis) [10]. A 120° magnetic structure is formed by the spins in the ab-plane, because the inter-chain exchange interaction is antiferromagnetic. On applying magnetic fields parallel to the c-axis, the magnetization curve shows a jump at $H_J\sim$12.5 T [11] due to a quantum effect investigated by Nikuni and Shiba [12]. In contrast, in magnetic fields perpendicular to the c-axis, the helical structure gradually changes with increasing magnetic fields, and the spiral vector becomes constant at 11 T $< H <$ 13 T [13], corresponding to the magnetization plateau region in the magnetization curve [11]. These findings are caused by the quantum effect and the DM interaction. In chiral magnets with cubic symmetry such as MnSi [14], Fe$_{1-x}$Co$_x$Si [15], and Co$_2$OSeO$_3$ [16], a topological defect in spin arrangement, the so-called Skyrmion lattice, was observed at around the magnetic ordering temperature in a finite magnetic field.

The title chiral magnet CrNb$_3$S$_6$, which belongs to the hexagonal space group $P6_322$ [17], shows a remarkable feature in magnetic fields perpendicular to the c-axis. The crystal structure of CrNb$_3$S$_6$ is a layered 2H-type NbS$_2$ intercalated by Cr atoms, and the lattice constants are $a = 5.75$ Å and $c = 12.12$ Å [18]. The Curie-Weiss (CW) temperature Θ of this sample is 145 K (ferromagnetic), and a sharp anomaly in the temperature dependence of magnetization, indicating magnetic ordering, was observed at 127 K [18]. From the analyses of the magnetization and neutron diffraction measurements, the magnetic structure of CrNb$_3$S$_6$ was determined to be helical with a long period of helicity since the wave vector of the helix is $Q = 480$ Å [17, 18]. On applying magnetic fields perpendicular to the c-axis, the spiral structure winds down periodically, and the magnetic structure with alternate ferromagnetic and spiral domains, the so-called chiral soliton lattice (CSL), emerges. The CSL in CrNb$_3$S$_6$ has already been observed by a Lorentz transmission electron microscopy [19], and it revealed that the length of the ferromagnetic domain of the CSL state becomes long with increasing magnetic field, and finally the system achieves the field-induced ferromagnetic phase above $H_s \sim$ 2.3 kOe [19]. This feature in CrNb$_3$S$_6$ is very unusual and may be applied to future electronic devices. In contrast, the magnetization curve for the magnetic field parallel to the c-axis shows a linear increase up to about 2 T as expected for the magnetic field perpendicular to the spiral plane.

In this paper, we report on the results of electron spin resonance (ESR) measurements performed for the evaluation of the exchange and the DM constants in CrNb$_3$S$_6$.

2 Experimental details

Single crystal samples of $CrNb_3S_6$ were synthesized by a chemical transport method, and the details of the synthesis are described in Ref. [18]. Our electron spin resonance (ESR) measurement system consists of a home-made ESR cryostat, a superconducting magnet (Oxford Instruments, 14 T at 4.2 K), a vector network analyzer MVNA (ABmm), and a Lock-in-amplifier (Seiko Instruments). In ESR measurements at 20.0, 24.7, and 27.6 GHz, we used a cylindrical cavity resonator (at 20.0 and 24.7 GHz, Teflon cylinders were inserted inside the resonator, and at 27.6 GHz, no Teflon cylinder was inserted inside the resonator.). The external magnetic field H_{ext} is applied to the c-axis of $CrNb_3S_6$ and is perpendicular to the microwave oscillating magnetic field H_{mw}.

3 Results and Discussion

Figure 1(a) shows ESR spectra of a single crystal of $CrNb_3S_6$ at $T = 1.5$ K for $H_{ext}//c$-axis and $H_{mw} \perp c$-axis. We observed some ESR absorption signals at each frequency, and each symbol indicates a resonance point. The intensity of the ESR signals at 27.6 GHz in low magnetic fields are comparatively weak, and we think this observation results from an ESR branch that is almost independent of the magnetic field. Figure 1(b) shows the frequency-magnetic field diagram, and we plot the resonance fields with the same symbols used in Fig. 1(a). In previous magnetization measurements in magnetic fields parallel to the c-axis, the magnetization increases almost linearly and saturates around 2 T [18]. Indeed, the ESR branches above the saturation also increase linearly with respect to the magnetic field. Therefore, we fitted these ESR branches above 2 T indicated by open squares and crosses with linear lines as shown in Fig. 1(b). At $f = 0$, the fitted line on the squares reaches 2.31 T, which is very close to the saturation field. Thus, comparing this observation with the magnetization result, we define $H_s = 2.31$ T as the saturation field in this paper [18, 19].

We now focus on the ESR branches below H_s. From neutron scattering measurements, the magnetic structure of $CrNb_3S_6$ at zero magnetic field is determined to be helical with spins lying in the ab-plane [17, 18]. On applying the magnetic field parallel to the c-axis, spins lean towards the c-axis, and a cone-like structure appears at $0 < H < H_s$. In this field range, Kishine and Ovchinnikov [20] calculated ESR mode by means of a spin wave theory. Thus, we analyze the observed ESR branch ν_q below H_s given by

$$\frac{h\nu_q}{2\tilde{J}S} = \sqrt{\left[1 - \cos(qc_0)\right]\left[\overline{\lambda} - \overline{\gamma}\cos(qc_0)\right]} , \quad (1)$$

where h is Planck's constant, $\tilde{J} = \sqrt{\left(J_1^2 + D^2\right)}$ (the ferromagnetic exchange constant $J_1 = 3J$ (> 0) and the DM constant D), $S = 3/2$ the spin quantum number, $q = 2\pi/L(0)$ the wave number ($L(0) = 480$ Å, the spiral length obtained from Lorentz TEM measurements [19]), $c_0 = 6.06$ Å the distance between the nearest magnetic moments along the c-axis. The magnetic field dependent parameters are represented as $\overline{\lambda} = 1 + \left(K_\perp/\tilde{J}\right)\sin^2\theta_0$ and $\overline{\gamma} = (J_1/\tilde{J})\sin^2\theta_0 + \cos^2\theta_0$ in which $K_\perp$ (> 0) represents the easy-plane anisotropy constant, and the cone angle $\theta_0 = \cos^{-1}(H/H_s)$ [20].

In considering the aforementioned parameters, there are not enough data points to determine J, D, and $K_\perp$. Therefore, we tried to refine the eq. (1) by using the results of previous measurements. First, we note the relation between J and D. The pitch angle φ in the helical magnetic structure is written as $\varphi = \tan^{-1}(D/J)$ and is determined from the values of $L(0)$ and c_0 to be $\varphi = 360° \times c_0/L(0) \sim 4.55°$ [17-19]. From these equations, we evaluate the ratio D to J. Next, we evaluate the $K_\perp$ from the saturation field. The saturation field is represented as $g\mu_B H_s = 2S(\tilde{J} - J_1 + K_\perp)$ according to Kishine's theory [20].
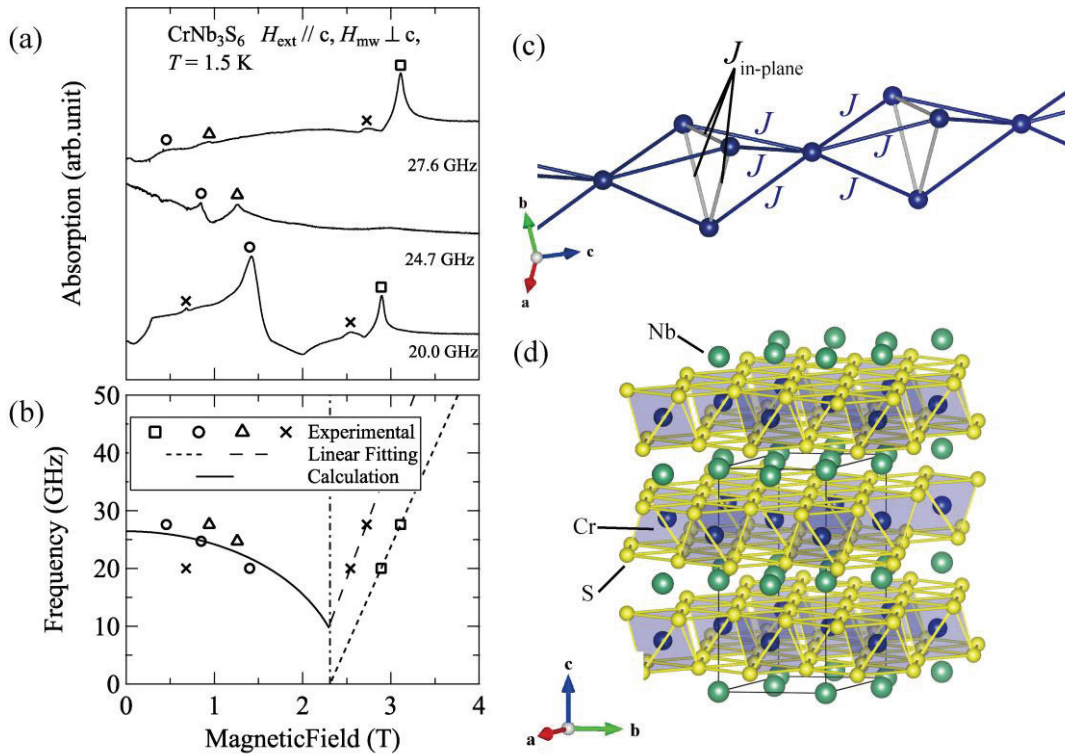
Figure 1: (a) ESR spectra of a single crystal of $CrNb_3S_6$ at designated frequencies. Magnetic field is applied parallel to the c-axis. Symbols indicate ESR resonance fields. (b) Frequency vs. magnetic-field plot of the resonance fields. The solid line indicates a result of fitting by using eq. (1). The dashed and broken lines are the results of the linear-line fitting of open squares and crosses, respectively. The dash-dotted vertical line is the expected saturation field. (c) Chain structure of Cr^{3+} ions and the exchange pathways. (d) Crystal structure of $CrNb_3S_6$. The chains run along the c-axis. Each Cr^{3+} ion is surrounded by sulfur octahedron, and Cr^{3+} ions form a triangular lattice in the ab-plane.

In our analysis, we set the g-value as $g=2.00$, because each Cr^{3+} ions is surrounded by sulfur octahedron as shown in Fig. 1(d) and then the orbital singlet state turns to be the ground state, resulting in the g-value of Cr^{3+} ion close to the g-value of free electron g_e. Accordingly, we can evaluate the value of $K_\perp$ from J and H_s, because $\tilde{J}$ is represented as a function of J. Then, we fit the ESR points below H_s indicated by the open circles to eq.(1) as shown with the solid line in Fig. 1 (b). From the fit, we obtain the parameter values $J/k_B=16.2$ K, $D/k_B=1.29$ K, and $K_\perp/k_B=1.02$ K. In this fitting, however, we neglect the resonance points indicated by the triangles, because only one theoretical ESR branch is calculated by Kishine and Ovchinnikov [20].

First, we discuss the magnitude of the evaluated ferromagnetic exchange constant. The CW temperature of $CrNb_3S_6$ is $\theta_{CW} \sim 145$ K [18], but the evaluated ferromagnetic exchange constant ($J/k_B = 12.0$ K) is about one tenth smaller than θ_{CW}. Hence, we assume that the spins in the ab-plane are strongly coupled ferromagnetically as discussed by Miyadai *et al.* [18], and such planes are coupled with each other by weak ferromagnetic interactions corresponding to the evaluated J value. Taking a closer look at the crystal structure of $CrNb_3S_6$ shown in Fig. 1(d), we see the nearest neighbor Cr^{3+} ions form a triangular lattice in the ab-plane. If the exchange interactions between these

Cr^{3+} ions are antiferromagnetic, we would probably observe different magnetic behavior caused by geometrical frustration. Moreover, the magnetization curve of $CrNb_3S_6$ for $H_{ext} \perp c$ shows a very low saturation field ~0.15 T [18]. Therefore, we think that our assumption is applicable for this compound. Quite recently, Shinozaki *et al.* calculated the magnetic field and the temperature dependences of magnetization using mean-field analysis and classical Monte Carlo simulation at finite temperatures [21]. Their calculated magnetization curves are qualitatively consistent with those observed in experiments. The evaluated parameter values are $J/k_B = 8.2$ K (ferromagnetic) and, $D/k_B = 1.3$ K, which are not far from our evaluated values. In addition to these values, they also evaluated the in plane exchange constant and obtained $J_{in-plane}/k_B = 67$ K (ferromagnetic) by the Monte Calro simulation. This result is consistent with our assumption.

Next, we discuss ESR branches at $0 < H < H_s$. As shown in Fig. 1(b), we observed two ESR branches in this region. However, only one ESR branch was derived from a simple one-dimensional chiral spin wave theory [20]. In MnSi in which a probable ferromagnetic exchange interaction and a DM interaction cause a helical spin structure, two ESR branches were observed at $0 < H < H_s$ [22]. These two branches were interpreted as helical spin resonance modes based on Yoshimori's theory [23] for a symmetric helimagnet. Two ESR branches below the saturation field were well-fitted by the NN ferromagnetic and NNN antiferromagnetic exchange interaction model, which was developed by Copper and Elliott [24, 25]. However, MnSi is a chiral helimagnet, and thus this symmetric helimagnet model is not applicable. We need to devise resonance modes for the chiral magnet $CrNb_3S_6$ as well as MnSi beyond the simple one-dimensional spin wave model.

Finally, we discuss the ESR branches at $H > H_s$. As mentioned above, this field region is the field induced ferromagnetic phase. We observed two linear ESR branches above H_s. In MnSi, the ESR branch above H_s has the finite positive intercept on the frequency axis [22] due to the ferromagnetic resonance mode. $CrNb_3S_6$ is a similar chiral magnet to MnSi, but the ESR branches at $H > H_s$ do not extrapolate to the positive intercept on the frequency axis in the frequency-field plane. The higher field ESR branch extrapolates to the saturation field H_s and the other branch does not. The difference in ESR branches above H_s between $CrNb_3S_6$ and MnSi is interesting, but the reason for this difference is unclear at present.

4 Conclusions

In conclusion, we have performed ESR measurements of a single crystal of the chiral helimagnet $CrNb_3S_6$ in magnetic fields parallel to the c-axis. We observed some ESR absorption signals at $20 < f < 30$ GHz. From the analysis using the resonance mode calculated by Kishine and Ovchinnikov, we obtain the parameter values $J/k_B = 16.3$ K, $D/k_B = 1.29$ K, and $K_\perp/k_B = 1.02$ K. The evaluated ferromagnetic exchange constant is much smaller than that obtained from the Curie-Weiss (CW) temperature. This result is a consequence of the in-plane ferromagnetic interaction being comparable to this CW temperature. We observed two ESR branches at $0 < H < H_s$, and this observation contradicts the finding of only one ESR branch calculated using spin wave theory applied to the one dimensional chiral magnet, indicating a more applicable theory appropriate for $CrNb_3S_6$ is required. The ESR branches at $H > H_s$ are not explained by the field induced ferromagnetic resonance modes observed in MnSi. These findings remain to be solved in our future study.

Acknowledgement

References

[1] T. Kimura, T. Goto, H. Shintani, K. Ishizaka, T. Arima and Y. Tokura, Nature **426**, 55 (2003).

[2] M. Kenzelmann, A. B. Harris, S. Jonas, C. Broholm, J. Schefer, S. B. Kim, C. L. Zhang, S. W. Cheong, O. P. Vajak and J. W. Lynn, Phys. Rev. Lett. **95**, 087206 (2005).

[3] S. Park, Y. J. Choi, C. L. Zhang and S-W. Cheong, Phys. Rev. Lett. **98**, 057601 (2007).

[4] Y. Naito, K. Sato, Y. Yasui, Y. Kobayashi, Y. Kobayashi and M. Sato, J. Phys. Soc. Jpn. **76**, 023708 (2007).

[5] H. Katsura, N. Nagaosa and A. V. Balatsky, Phys. Rev. Lett. **95**, 057205 (2005).

[6] B. J. Gibson, R. K. Kremer, A. V. Prokofiev, W. Assmus and G. J. McIntyre, Physica B **350**, e253 (2004).

[7] Y. Kobayashi, K. Sato, Y. Yasui, T. Moyoshi, M. Sato and K. Kakurai, J. Phys. Soc. Jpn. **78**, 084721 (2009).

[8] R. M. Bozorth and C. D. Graham Jr., G. E. Tech. Inf. Series 66-C-225 (1966).

[9] A. W. Schlueter, R. A. Jacobson and R. E. Rundle, Inorg. Chem. **5**, 277 (1966).

[10] K. Adachi, N. Achiwa and M. Mekata, J. Phys. Soc. Jpn. **49**, 545 (1980).

[11] M. Mino, K. Ubukata, T. Bokui, M. Arai, H. Tanaka and M. Motokawa, Physica B **201**, 213 (1994).

[12] T. Nikuni and H. Shiba, J. Phys. Soc. Jpn. **62**, 3268 (1993).

[13] A. Hoser, N. Stüßer, U. Schotte and M. Meißner, Appl. Phys. A **74**, S707 (2002).

[14] S. Mühlbauer, B. Binz, F. Jonietz, C. Pfleiderer, A. Rosch, A. Neubauer, R. Georgii and P. Böni, Science **323**, 915 (2009).

[15] X. Z. Yu, Y. Onose, N. Kanazawa, J. H. Park, J. H. Han, Y. Matsui, N. Nagaosa and Y. Tokura, Nature **465**, 901 (2010).

[16] S. Seki, X. Z. Yu, S. Ishiwata and Y. Tokura, Science **336**, 198 (2012).

[17] T. Moriya and T. Miyadai, Solid State Commun. **42**, 209 (1982).

[18] T. Miyadai, K. Kikuchi, H. Kondo, S. Sakka, M. Arai and Y. Ishikawa, J. Phys. Soc. Jpn. **52**, 1394 (1983).

[19] Y. Togawa, T. Koyama, K. Takayanagi, S. Mori, Y. Kousaka, J. Akimitsu, S. Nishihara, K. Inoue, A. S. Ovchinnikov and J. Kishine, Phys. Rev. Lett. **108**, 107202 (2012).

[20] J. Kishine and A. S. Ovchinnikov, Phys. Rev. B **79**, 220405 (2009).

[21] M. Shinozaki, S. Hoshino, J. Kishine, K. Hukushima, Y. Kato, and M. Takashi, preprint.

[22] M. Date, K. Okuda and K. Kadowaki, J. Phys. Soc. Jpn. **42**, 1555 (1977).

[23] A. Yoshimori, J. Phys. Soc. Jpn. **14**, 807 (1959).

[24] B. R. Copper, R. J. Elliott, S. J. Nettel and H. Suhl, Phys. Rev. **127**, 57 (1962).

[25] B. R. Copper and R. J. Elliott, Phys. Rev. **131**, 1043 (1963).